Dynamics of a Phobos-anchored tether near the L1 libration point

Vladimir S. Aslanov
Samara National Research University, 34, Moscovskoe shosse, Samara 443086, Russia
+7-9276889791
aslanov_vs@mail.ru
http://aslanov.ssau.ru/

Abstract The paper focuses on the development of a new mission to explore Phobos using an anchored tether system located below the L1 Mars-Phobos libration point and deployed toward Mars at a length slightly greater than the distance from Phobos. The basic assumptions in terms of a planar circular restricted three-body problem are formulated. The motion equations are derived in polar coordinates relative to the anchor point of the tether system. For a constant-length tether, an energy integral, equilibrium positions, and phase portraits for various anchored point locations on the Phobos surface are found. Analytical formulas for the tether tension force are derived and the influence of system parameters on this force is investigated for static and dynamic cases. To provide asymptotic Lyapunov stability of the tether in the vicinity of equilibrium positions, the feedback control is proposed. To validate the obtained results, numerical simulation of the space tether system controlled motion taking into account the eccentricity of the Mars-Phobos orbit using the equations in Nechvile's variables is performed. Results of this simulation confirm the results obtained earlier. Conclusions about the feasibility of the implementation of the suggested mission and features of the behavior of the tether system using the proposed feedback control are made. The results of this study can be used to enable many future missions throughout the solar system.

Keywords *Anchored tether · L1 libration point · Phobos surface · Oscillation stability ·Feedback control*

1 Introduction

The restricted three-body problem is the foundation for solving many applied problems of astronautics, in particular, for the computation of interplanetary flights. A detailed analysis of main studies on this topic can be found in the Szebehely's textbook [1]. Currently, a large number of papers on the restricted three-body problem have been published (eg. [2-8]), in which this problem is studied in detail, and these results are widely used in various astronautical missions. Equilibrium points or libration points in the circular restricted three-body problem represent a unique phenomenon in astrodynamics. In the Mars-Phobos system L1 and L2 collinear libration points have two additional special properties, allowing, among other tasks, a relatively simple to study of the Phobos surface. First, Phobos does not rotate relative to the line connecting the centers of mass of Mars and Phobos, on which the L1 and L2 libration points are located. Second, the L1 and L2 libration points are located above the Phobos surface at a distance of about 3.4 km. Such a short distance allows to use the space tether systems technology to organize a transport channel between the Phobos surface and the L1/L2 libration point. It remains only to choose the attachment point of the tether system: at the L1 libration point or on the Phobos surface. The scientific interest and complexity of the problem lies in the fact that the gravitational force of two large bodies (primaries) and the centrifugal force of inertia caused by the rotation of the Mars-Phobos system act on the tether system, located near the L1/L2 libration point. In such cases, it is most convenient to use mathematical models developed within the restricted three-body problem, improving them to describe the tether system. The field of space tethers has received very much attention in recent decades, with several books [9–12] and many papers [13–36] available in the scientific literature. The tether systems can emerge as a new technology for developing the planets of the solar system, their moons [24], and the exploitation of other celestial bodies as well as asteroids [21].

In 2017, NASA proposed the PHLOTE mission (Phobos L1 Operational Tether Experiment) to explore the surface of Phobos utilizing a tether system ‘‘anchored’’ at the L1 libration point [24]. As a release point of the tether, it was proposed to use an orbiting spacecraft, which should hover in the vicinity of the L1 libration point of the Mars-Phobos system. An alternative (or development) to the PHLOTE mission could be a tether system anchored on the Phobos surface, the end mass of which is located slightly above the L1/L2 libration point. An anchored tether on the far side of Phobos (with respect to Mars) to deploy tethered sensors was first proposed in [9, 25]. In 2012, a Phobos-anchored Mars Space Elevator is discussed in [26].

The development of effective tether system control laws and algorithms is one of the key issues in the development of missions using space tether systems. Li and Zhu [27] examined the control of the geometric profile of an electrodynamic tether by means of simulated predictive control using an induced electric current in the tether. Ref. [28] aimed at developing effective angular velocity observers for a space tether system using unit vector measurements along a tether. A new methodology for on-line inertia parameters estimation for a rigid space body captured by a tethered system is discussed in [29]. Ref. [30] develops a dynamic model with high accuracy and precision to investigate the suppression of partial space elevator libration caused by a moving climber by deploying and/or retrieving a tether on the main and subsatellites. Zhang and Huang [31] proposed a new underactuated tethered satellite system controller for both deployment and retrieval. This control scheme makes the best use of the dynamic characteristics of the tethered system. Krupa et al. [32] considered new optimal control strategies for the processes of deployment or retrieval of one satellite from or to another satellite. Tethered slingshot maneuver in the restricted elliptical three-body problem to change a spacecraft orbit, in which the tether attached to a celestial body makes a rotation in a velocity vector of the spacecraft was studied in detail by Ferreira et al. [33]. The paper by Jung et al. [34] presents a dynamic analysis of a tethered satellite system with a moving mass. N-star general dynamic model of a tethered satellite system with a closed-loop configuration was presented Zhu et al. [35]. Yu et al. [36] focused on a global dynamics of linear tethered satellite formation and, in particular, studied in detail an influence of initial states of the system on the motion shapes and their critical values.

The paper focuses on the development of a new mission to explore Phobos using an anchored tether system located below the L1 Mars-Phobos libration point and deployed toward Mars at a length slightly greater than the distance from Phobos. The purpose of the paper is to demonstrate the possibility of using the anchored tether system tether system for the study of Phobos. To achieve this purpose, a mathematical model of a planar motion of the anchored tether system is developed and a simple law of stabilization of the tether system is proposed. The influence of the tether length, the position of the attachment point on the Phobos surface and other parameters on the behavior of the tether system is studied. This is the first preliminary study of the possibility of implementing a mission using a tether system "attached" on the Phobos surface under the libration point L1. The main contribution of the paper is that, based on simplified mathematical models and using the classical methods of Lyapunov's stability theory, the possibility of using a tether system near the Libration point to study Phobos is demonstrated.

Initially, the basic assumptions in terms of a planar circular restricted three-body problem are formulated, and the motion equations are derived in polar coordinates relative to the anchor point of the tether system. Next, for a constant-length tether, an energy integral, equilibrium positions, and phase portraits for various anchored point locations on the Phobos surface are found. After that, analytical formulas for the tether tension force are derived and the influence of system parameters on this force is investigated for static and dynamic cases. The next stage is devoted to the development of feedback control, which would provide asymptotic Lyapunov stability of the tether in the vicinity equilibrium position. Further, to validate the obtained results, a mathematical model is built using Nechvile's variables, which takes into account the eccentricity of the Mars-Fobos orbit. Numerical simulations of the mathematical model confirm the results obtained earlier.

Finally, conclusions about the feasibility of the implementation of the suggested mission and features of the behavior of the tether system using the proposed feedback control are made.

2 Motion equations of the anchored tether within the context of the circular restricted three-body problem

In this section to better understand the behavior of the Phobos-anchored tether system under the gravity of the two primaries A_1 and A_2 (Mars-Phobos), and the centrifugal force in the rotating Mars-Phobos frame the motion equations of the end mass C are considered within the context of the planar circular restricted three-body problem [1]. It is assumed that the end body C is many times less than the mass of the bodies A_1 and A_2. Therefore, the body C has negligible effect on the other bodies. It all helps to determine equilibrium positions, to find a period of oscillations and to identify some other regularities of motion of a peculiar pendulum in the two-body gravitational field and under the centrifugal force.

2.1 Key assumptions

We introduce acceptable assumptions that do not distort a principled picture of the proposed Phobos-anchored tether mission (PATM):

1) It is supposed that the Mars and Phobos move in elliptical orbits around their mutual mass center. In reality, the orbits have a small eccentricity $(e = 0.0151)$, and this will be taken into account in verifying the main results by numerical simulations.

2) The mass m of the point C attached to the tether is significantly less than the primaries' masses m_1 and m_2

$$m \ll m_2 < m_1 \qquad (1)$$

3) The tether is inextensible and weightless rigid rod. This suggests that the developed mathematical models and the obtained solutions are valid only in the case of a stretched tether.

4) In all considered cases, only in-plane motion is studied.

5) This paper studies the influence of displacement relative to the gravitational vertical Ox (Fig.1) of the anchoring point of the tether system on the Phobos surface on the tether system motion near the L1 libration point. The largest Stickney Crater on Phobos [37, 38] always faces Mars due to Phobos' synchronous rotation and locates under the L1 libration point. The digital terrain model (DTM) profile of this crater has a rather complex configuration (Fig. 2), so at this initial stage of the study it is approximated by a straight line perpendicular to the gravitational vertical at a transverse displacement within ± 1.5 km. This makes it easy to set the coordinates of the tether anchor point.

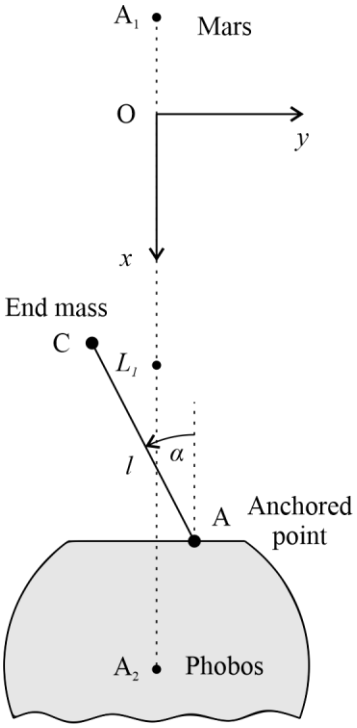

Fig. 1 The frame Oxy and the polar frame (l, α)

a

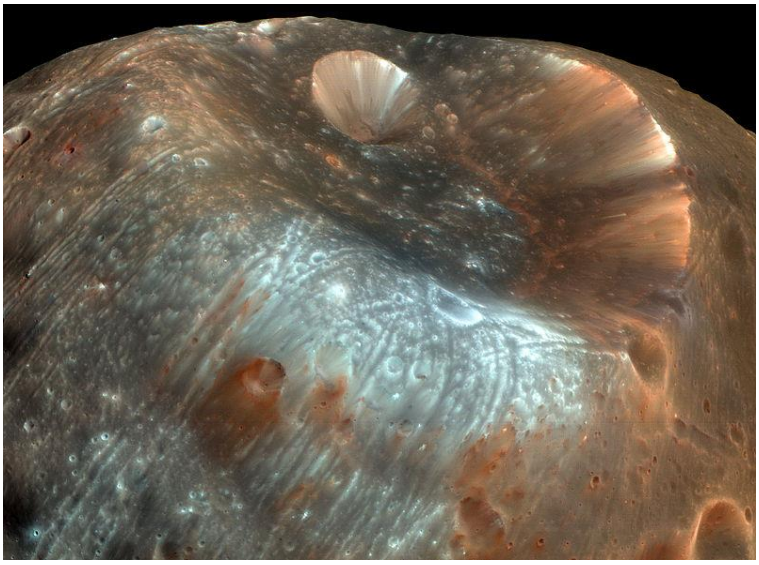

b

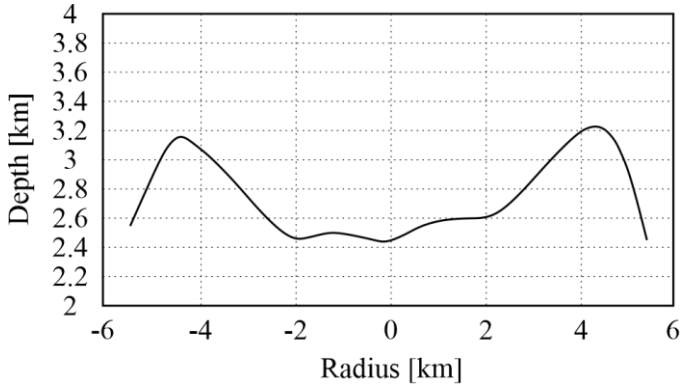

Fig. 2 a Stickney crater and its DTM profile **b** [38]

The accepted assumptions will be used to develop a mathematical model.

2.2 Motion equations in polar coordinates relative to the anchor point

Consider the equations of the end mass planar motion in the Local-Vertical-Local-Horizontal frame Oxy within the scope of the classical restricted three-body problem [1, 39]

$$\ddot{x} = \frac{\partial W}{\partial x} + n^2 x + 2n\dot{y} - \frac{1}{m} T_x \tag{2}$$

$$\ddot{y} = \frac{\partial W}{\partial y} + n^2 y - 2n\dot{x} - \frac{1}{m} T_y \tag{3}$$

where n is mean orbital rate, $\mathbf{T} = \left(T_x, T_y\right)$ is the tether tension force acting on the end mass from the tether. The potential of Eqs. (2) and (3) is written as

$$W(x, y) = G\left(\frac{m_1}{r_1} + \frac{m_2}{r_2}\right) \tag{4}$$

where G is Newtonian gravitational constant, the distance between the primary 1 and the end mass

$$r_1 = \sqrt{(x + p\mu)^2 + y^2} \tag{5}$$

the distance between the primary 2 and the end mass

$$r_2 = \sqrt{(x - p(1-\mu))^2 + y^2} \tag{6}$$

where $\mu = \frac{m_2}{m_1 + m_2}$ is the mass ratio; p is the distance between the primaries 1 and 2.

Position of the end mass C relative to the anchoring point A in the polar frame (l, α) is defined by substituting the variables (Fig. 1)

$$x = a_x - l\cos\alpha, \quad y = a_y - l\sin\alpha \tag{7}$$

where (a_x, a_y) are the coordinates of the anchoring point A in the frame Oxy. In the polar reference frame (l, α) Eqs. (2) and (3) can be written as

$$\ddot{\alpha} + F_\alpha = 0 \tag{8}$$

$$\ddot{l} + F_l = -\frac{1}{m} T \tag{9}$$

where m is the end body mass, $T = \sqrt{T_x^{\,2} + T_y^{\,2}}$ is the tether tension force acting on the end mass from the tether, T_x, T_y are the coordinates of the anchoring point A in the frame Oxy.

$$F_\alpha = \frac{n^2}{l}\left(a_y\cos\alpha - a_x\sin\alpha\right) - \frac{G}{l}\left(\frac{\left(-\left(p\mu + a_x\right)\sin\alpha + a_y\cos\alpha\right)m_1}{r_1^3} + \frac{\left(-\left(p\left(-1+\mu\right) + a_x\right)\sin\alpha + a_y\cos\alpha\right)m_2}{r_2^{\,3}}\right) \tag{10}$$

$$F_l = n^2\left(\left(a_x\cos\alpha + a_y\sin\alpha\right) - l\right) - l\dot{\alpha}\left(2n + \dot{\alpha}\right) - \frac{G}{l}\left(\frac{\left(a_y\sin\alpha + \left(a_x + p\mu\right)\cos\alpha - l\right)m_1}{r_1^3} + \frac{\left(a_y\sin\alpha + \left(a_x + p\left(-1+\mu\right)\right)\cos\alpha - l\right)m_2}{r_2^3}\right) \tag{11}$$

where the distance between the primary 1 and the end mass is

$$r_1 = \sqrt{\left(a_x + p\mu - l\cos\alpha\right)^2 + \left(a_y - l\sin\alpha\right)^2} \tag{12}$$

and the distance between the primary 2 and the end mass is

$$r_2 = \sqrt{\left(a_x + p\left(-1+\mu\right) - l\cos\alpha\right)^2 + \left(a_y - l\sin\alpha\right)^2} \tag{13}$$

For a constant tether length $l = const$ Eqs. (8) and (9) are reduced to one second-order differential equation for the tether deflection angle α

$$\ddot{\alpha} + F_\alpha = 0 \tag{14}$$

This equation has the following energy integral

$$\frac{\dot{\alpha}^2}{2} + U\left(\alpha\right) = E = const \tag{15}$$

where E is the total energy, the potential energy is

$$U\left(\alpha\right) = \int F_\alpha\left(\alpha\right) d\alpha = \frac{n^2}{l}\left(a_x\cos\alpha + a_y\sin\alpha\right) - \frac{G}{l^2}\left(\frac{m_1}{r_1} + \frac{m_2}{r_2}\right) \tag{16}$$

3 Phase portraits and bifurcation diagram

All phase portraits of the system (14) are plotted for the tether length

$$l = 3500\,m \tag{17}$$

Note that the distance between the Phobos surface and the L1 libration point is 3400m. Evolution of the phase portraits depending on the deflection of the tether anchoring points from the gravitational vertical can be observed in the Figs. 3-5, which show the dependence of the function (10) $F_\alpha\left(\alpha\right)$ and the phase portraits determined by Eq. (15). Consider the case when the anchoring point is located at the intersection of the gravitational vertical with the Phobos surface, and the transverse displacement is absent. Solving the equation

$$F_\alpha\left(\alpha\right) = 0 \tag{18}$$

for

$$a_y = 0 \tag{19}$$

on the interval $\left[-2\pi, 2\pi\right]$ one obtains the five stable equilibrium positions

$$\alpha_s = \left(-2\pi,\ -\pi,\ 0,\ \pi,\ 2\pi\right) \tag{20}$$

and the four unstable equilibrium positions (Fig. 3)

$$\alpha_{us} = \left(-5.437,\ -0.845,\ 0.845,\ 5.437\right) rad \tag{21}$$

a

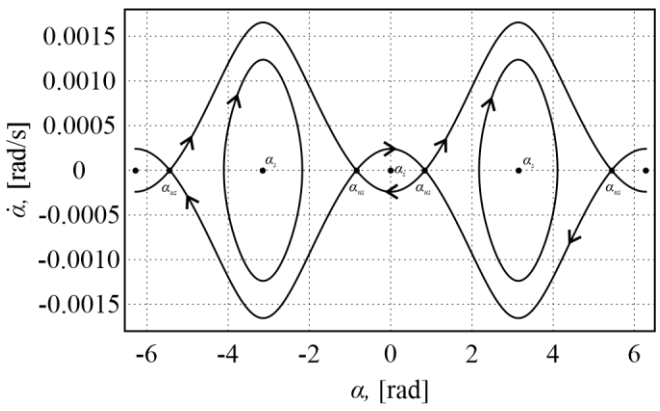

b

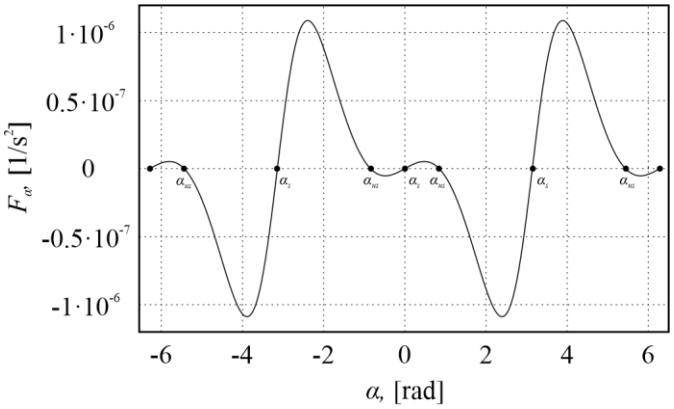

Fig. 3 **a** The function $F_\alpha(\alpha)$ and **b** the phase portrait $\dot{\alpha}(\alpha)$ for the tether length $l = 3500\,m$ and without the transverse displacement of the tether anchor point $a_y = 0$

As shown in Fig. 3, the phase portrait is symmetric with respect to the ordinate axis for the anchored tether without the transverse displacement. In the presence of the transverse displacement of the tether anchor point, the symmetry of the phase portrait is broken. For $a_y = 500\,m$ the stable equilibrium positions are

$$\alpha_s = (-6.147, -3.186, 0.137, 3.098)\,rad \tag{22}$$

and the unstable positions points are

$$\alpha_{us} = (-5.532, -0.922, 0.751, 5.361)\,rad \tag{23}$$

a

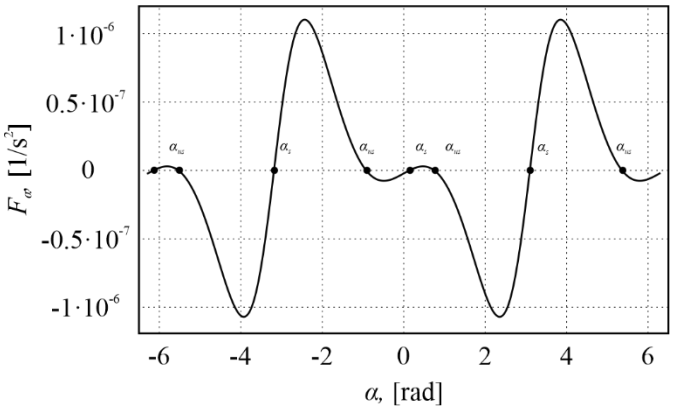

b

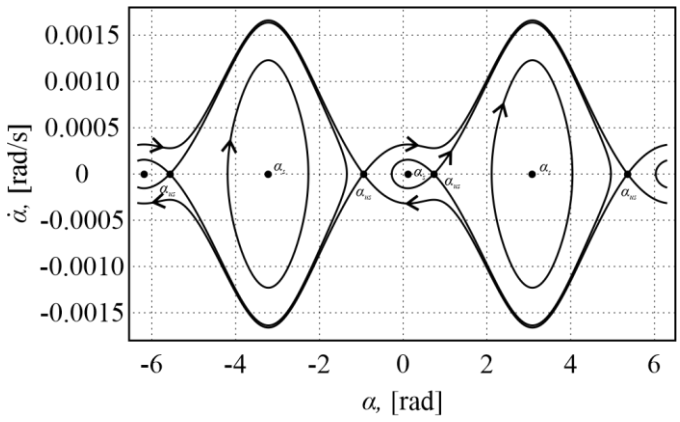

Fig. 4 **a** The function $F_\alpha(\alpha)$ and **b** the phase portrait $\dot{\alpha}(\alpha)$ for the tether length $l = 3500\,m$ and for the transverse displacement of the tether anchor point $a_y = 500m$

As the transverse displacement of the tether anchoring point increases, the central stable point ($\alpha_s = 0$) shifts the right. Under the following conditions:

$$F_\alpha(\alpha) = 0\,,\ \frac{\partial F_\alpha(\alpha)}{\partial \alpha} = 0 \qquad (24)$$

this point becomes neutral. A phenomenon known in non-linear dynamics as saddle-node bifurcation occurs, when two equilibria position collide and annihilate each other. For the tether length $l = 3500\,m$ it takes place in the case of the transverse displacement of the tether anchor point $a_y = 1164.6\,m$ (Fig. 5).

a

b

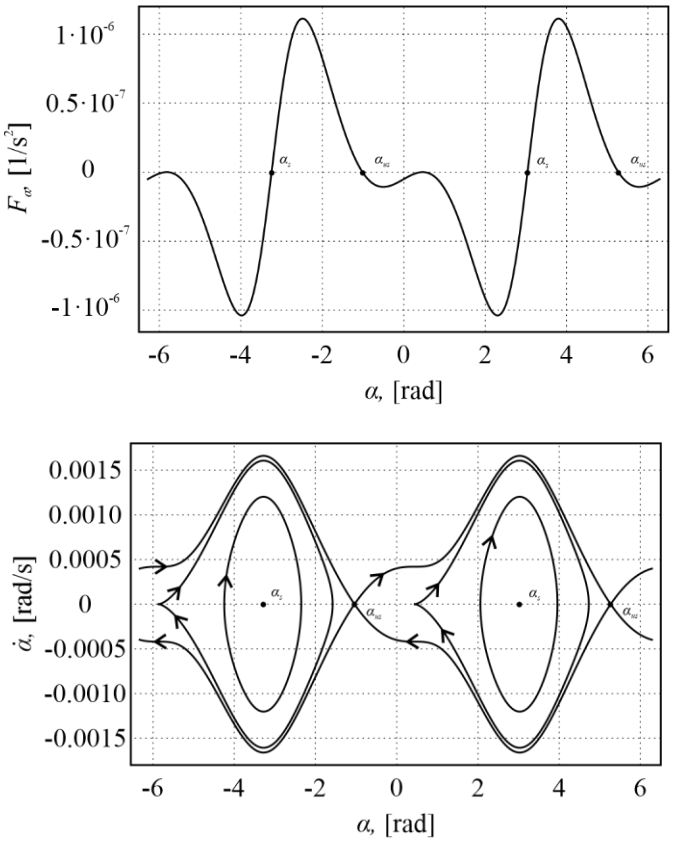

Fig. 5 **a** The function $F_\alpha(\alpha)$ and **b** the phase portrait $\dot{\alpha}(\alpha)$ for the tether length $l = 3500\,m$ and for the transverse displacement of the tether anchor point $a_y = 1164.6\,m$

A bifurcation diagram as a function of the transverse displacement of the tether anchor point is presented in Fig. 6 for the tether length $l = 3500\,m$. Solid lines in Fig. 6 correspond to stable equilibrium positions, and dashed lines indicate unstable positions. Two bifurcation values of the a_y parameter can be seen in the diagram $a_{y1} = -1164.6\,m$, $a_{y2} = 1164.6\,m$. The phase portrait corresponding to bifurcation value a_{y2} is shown in Fig. 5.

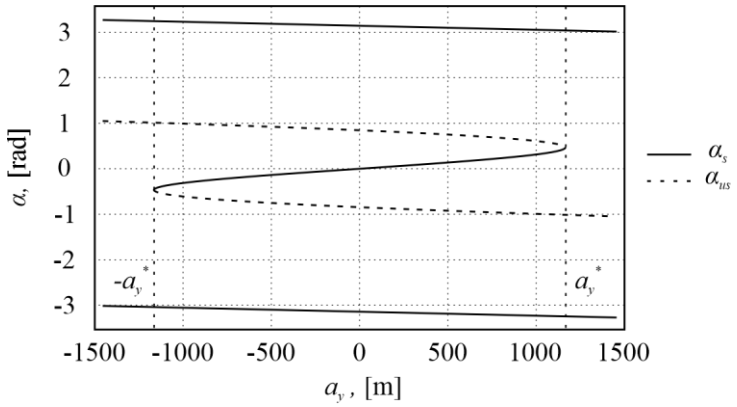

Fig. 6 Bifurcation diagram

4 Tether tension force

4.1 Static tension force of tether

Note that the above calculations are valid only for the stretched tether. Obviously, the anchored tether deployed along the gravitational vertical is stretched if its length is greater than the distance between the point L1 and the tether attachment point because the end mass is located above the point L1, as viewed from the side of the Phobos.

If the constant length tether is anchored without transverse displacement $(a_y = 0)$, then for the central stable point $(\alpha_s = 0, \dot{\alpha} = 0, \ddot{\alpha} = 0)$ the static tension force can be calculated using Eq. (9) according to the following formula

$$T_{st} = m n^2 \left(l - a_x\right) - mG\left[\frac{\left(a_x + p\mu - l\right)m_1}{\left(\left|a_x + p\mu - l\right|\right)^3} + \frac{\left(a_x + p\left(-1+\mu\right) - l\right)m_2}{\left(\left|a_x + p\left(-1+\mu\right) - l\right|\right)^3}\right] \tag{25}$$

For 5000kg end mass and the tether length 100 m longer than the distance between the L1 point and the Phobos surface ($3400\,m$) Eq. (25) gives the tension force of 0.23 N. If the excess is 1000 m, then the tension force is 2.2 N. Fig. 7 shows that the tension force of the deployed tether along the gravitational vertical from the Phobos surface increases almost directly proportional to its length, so for the end mass of 5000 kg and length of 5000 m the tension force is 3.4 N.

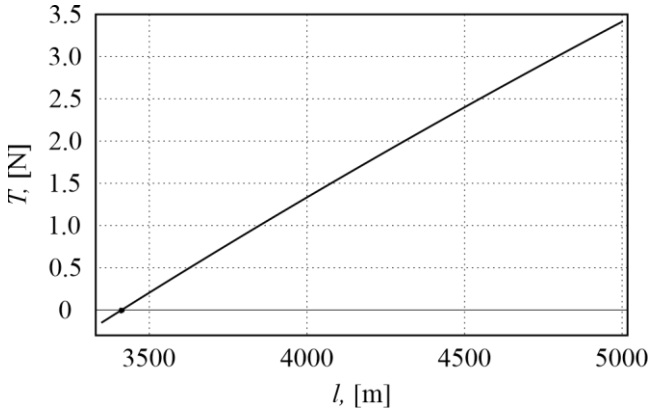

Fig. 7 The tension force of the vertically deployed tether from the surface of Phobos as a function of its length for the end mass (orbiter) equal to 5000 kg

In the conclusion here notice that if the tether is oscillating or/and is anchored with the transverse displacement, then the issue of its tension deserves a separate study.

4.2 Dynamic tension force of tether

The dynamic tether tension force can be found using Eqs. (9) and (11) as

$$T = -mF_l = -m\left[n^2 \left(\left(a_x \cos\alpha + a_y \sin\alpha \right) - l \right) - 2nl\dot{\alpha} - l\dot{\alpha}^2 - \right.$$
$$\left. \frac{G}{l}\left(\frac{\left(a_y \sin\alpha + \left(a_x + p\mu \right)\cos\alpha - l \right) m_1}{r_1^3} + \frac{\left(a_y \sin\alpha + \left(a_x + p\left(-1 + \mu \right) \right)\cos\alpha - l \right) m_2}{r_2^3} \right) \right] \qquad (26)$$

First, consider the case when the tether is anchored on the Phobos surface without the transverse displacement relative to the gravitational vertical $(a_y = 0)$. Figs. 8 and 9 show the tether tension force and the tether deflection angle from the gravitational vertical for the end mass of 5000 kg at different initial tether deflection angles and for different tether lengths: 3500 and 4500 m. Figs. 8(a), 9(a), and 10(a) depict thin horizontals with strokes to the outside $\left(\frac{\pi}{2}, -\frac{\pi}{2} \right)$, which mark the limits of possible tether oscillations due to the assumption of the surface topography of Phobos below the L1 libration point, as shown in Fig. 1.

a

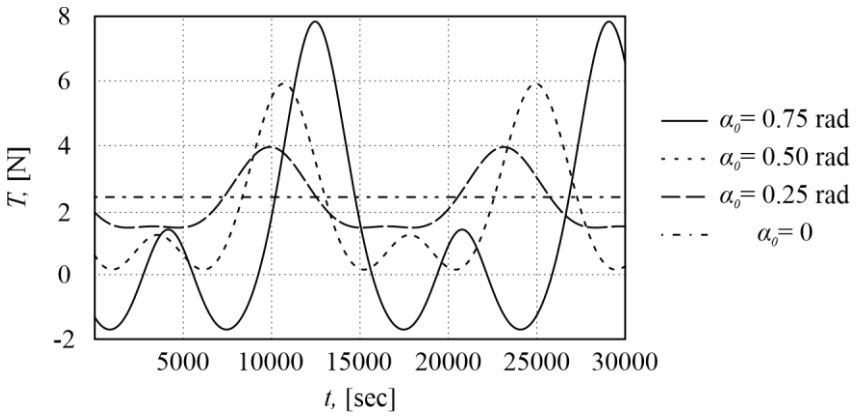

b

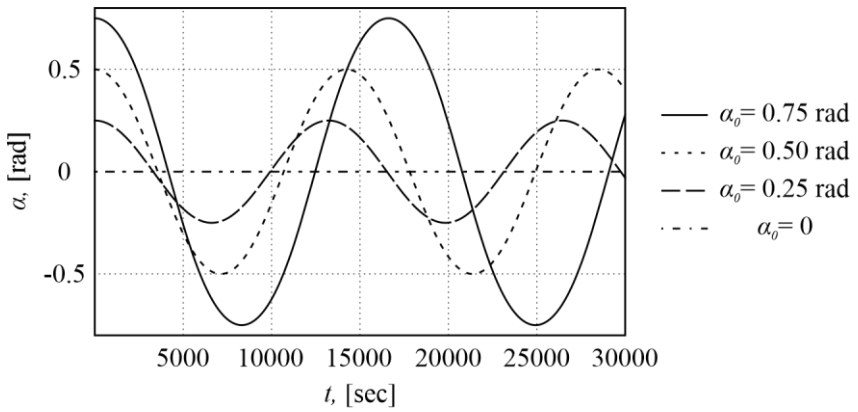

Fig. 8 a The tension force and **b** the tether deflection angle for the tether length 3500 m without the transverse displacement relative to the gravitational vertical $a_y = 0$

a

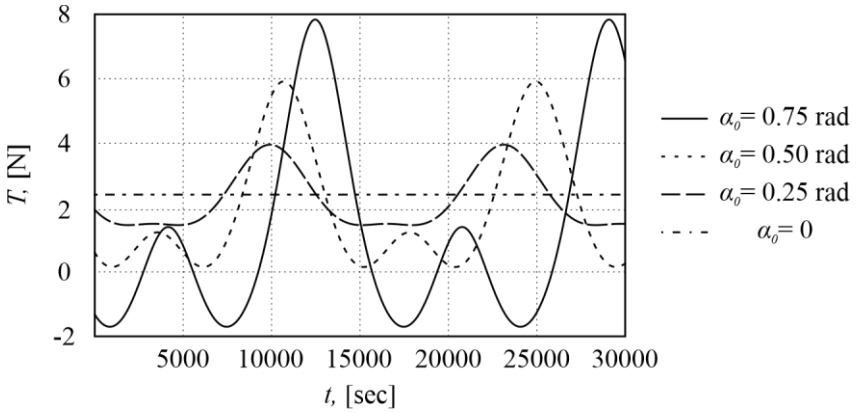

b

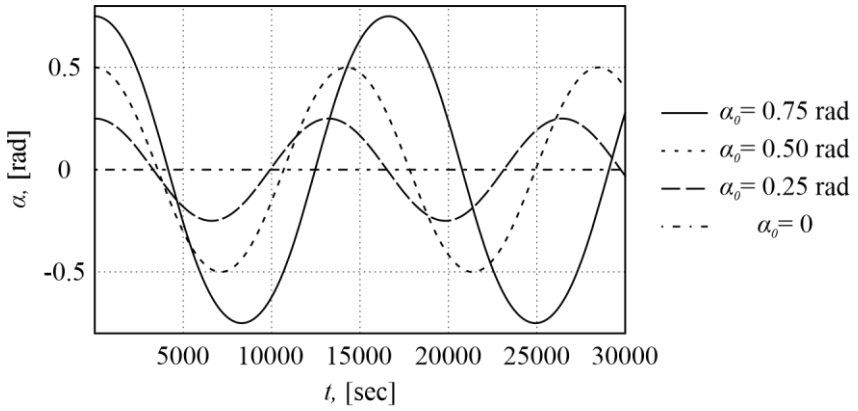

Fig. 9 a The tension force and **b** the tether deflection angle for the tether length 4500 m without the transverse displacement relative to the gravitational vertical $a_y = 0$

Fig. 10 shows the same as in Fig. 9 for the tether length 4500 m and with the transverse displacement relative to the gravitational vertical $a_y = 250\,m$, for which the stable position is different from zero and equal to $\alpha_s = 0.03 rad$.

a

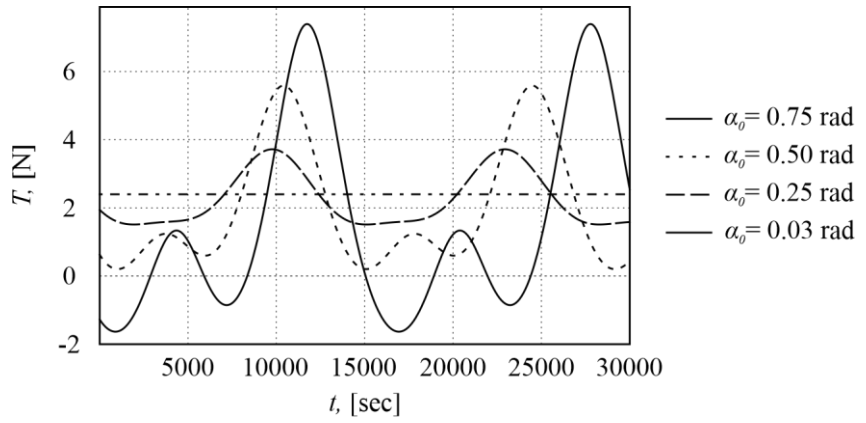

b

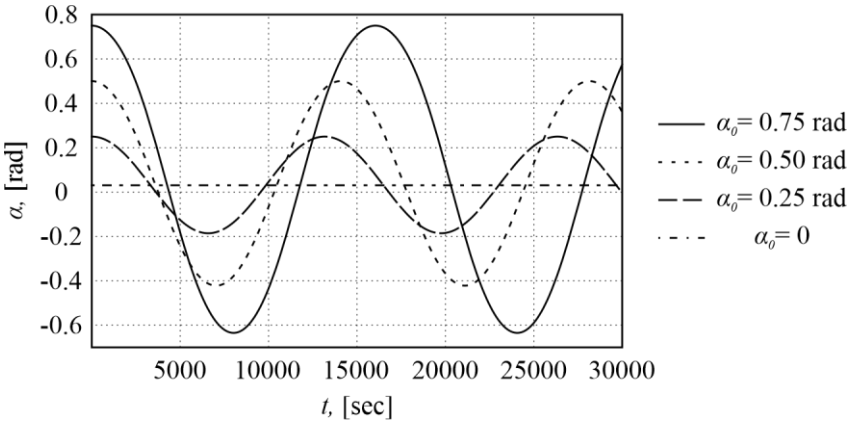

Fig. 10 **a** The tension force and **b** the tether deflection angle for the tether length 4500 m for the transverse displacement relative to the gravitational vertical $a_y = 250\,m$

By numerical simulation, let's estimate the contribution of the separate components of the tension force of the tether T (26). Three components can be distinguished: the gravitational force component T_{Gn}, the centrifugal inertial force component $T_{\text{centrifugal}}$, and the Coriolis force component T_{coriolis}.

$$T_{Gn} = -m\left[n^2 \left(\left(a_x \cos\alpha + a_y \sin\alpha \right) - l \right) - \frac{G}{l}\left(\frac{\left(a_y \sin\alpha + \left(a_x + p\mu \right)\cos\alpha - l \right) m_1}{r_1^3} + \frac{\left(a_y \sin\alpha + \left(a_x + p\left(-1+\mu\right)\right)\cos\alpha - l \right) m_2}{r_2^3} \right) \right] \quad (27)$$

$$T_{\text{centrifugal}} = ml\dot{\alpha}^2 \quad (28)$$

$$T_{\text{coriolis}} = 2mnl\dot{\alpha} \quad (29)$$

Obviously, according to (26)-(29) the following equality is always true

$$T = T_{Gn} + T_{\text{centrifugal}} + T_{\text{coriolis}} \quad (30)$$

Fig. 11 illustrates the contribution of each component of the tether tension force for the following parameters

$m = 5000\,kg, l = 4500\,m, a_y = 250\,m$

and the initial conditions

$\alpha_0 = 0.5\,rad, \dot{\alpha}_0 = 0$

a

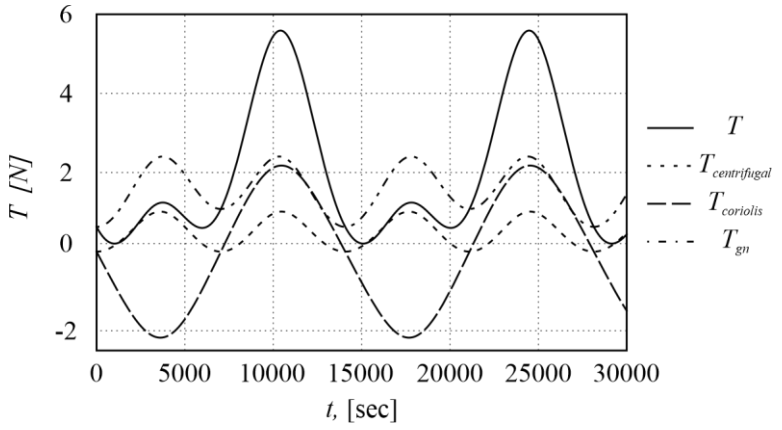

b

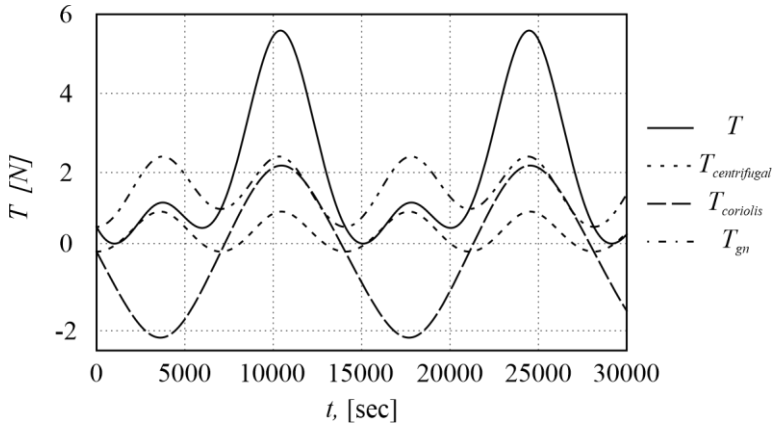

Fig. 11 **a** The tension force and **b** the tether deflection angle for the tether length 4500 m for the transverse displacement relative to the gravitational vertical $a_y = 250\,m$

According to the formulation of the problem, the simulation results presented above correspond to the physical process only when the tether is stretched ($T > 0$).
The graphs in Fig. 8-11 allows one to make some conclusions.
- The greater the amplitude of oscillation of the tether, the greater the period of oscillation.
- The greater the amplitude of oscillation and the length of the tether, the greater the tether tension force.
- According to the results of the numerical simulation shown in Fig. 11 and Eq. (29) a significant contribution to the tension force is made by the Coriolis force T_{coriolis}, which extends the tether at $\dot{\alpha} > 0$ and compresses the tether at $\dot{\alpha} < 0$.
- Figs. 9 and 10 show that a small displacement of the tether anchoring point from the gravitational vertical does not fundamentally change the tether tension force.

5 Feedback control development

The following feedback control developments all have the common goal to ensure the absence of oscillations of the tether system relative to a stable point, or in other words, to guarantee a asymptotic stability for all admissible variations. Consider only cases where a stable equilibrium position exists near the gravitational vertical, such as those shown in Figs. 3 and 4.
The following feedback control is proposed

$$u = -c_\omega \dot{\alpha} \tag{31}$$

where $c_\omega > 0$ is a constant rate feedback gain. This control law can be realized by thrusters of the orbiter, which is the end mass of the tether system. Then, taking into account Eq. (8) and the feedback control (31), the tether oscillation is described by the equation

$$\ddot{\alpha} + F_\alpha = u \tag{32}$$

where function F_α is determined Eq. (10).
To investigate the stability of the potential feedback control law in Eq. (31), the difference of the total energy and the potential energy calculated in stable equilibrium position U_s is used as a positive definite Lyapunov function candidate

$$V = \left[\frac{\dot{\alpha}^2}{2} + U(\alpha)\right] - U(\alpha_s) \tag{33}$$

or, according to Eq. (16)

$$V = \frac{\dot{\alpha}^2}{2} + \frac{n^2}{l}\left(a_x \cos\alpha + a_y \sin\alpha\right) - \frac{G}{l^2}\left(\frac{m_1}{r_1} + \frac{m_2}{r_2}\right) - U_s \qquad (34)$$

By definition, the difference $U(\alpha) - U(\alpha_s)$ is a non-negative value, therefore function (33) is definitely positive in the vicinity of the stable equilibrium position.

The derivative of the function (33) with respect to time using Eq. (32) is written as

$$\frac{dV}{dt} = \left(\ddot{\alpha} + \frac{dU}{d\alpha}\right)\dot{\alpha} = \left(\ddot{\alpha} + F_\alpha\right)\dot{\alpha} = u\dot{\alpha} \qquad (35)$$

If the constant rate feedback gain is positive ($c_\omega > 0$), then with the control law (31) is definitely negative

$$\frac{dV}{dt} = -c_\omega \dot{\alpha}^2 < 0 \qquad (36)$$

Thus, the system (32) is asymptotically stable according to Lyapunov. Fig. 12 illustrates the Lyapunov function (34) for the following parameters of the tether system and the control constant

$$l = 4500\,m, \quad a_y = 250\,m, \quad c_\omega = 0.01, \quad \alpha_s = 0.03\,rad \qquad (37)$$

Note that for the parameters (37) the five stable equilibrium positions exist on the interval $[-2\pi, 2\pi]$

$$\alpha_s = (-6.253, -3.121, 0.031, 3.121, 6.314)\,rad \qquad (38)$$

and the four unstable equilibrium positions

$$\alpha_{us} = (-5.437, -1.107, 1.058, 5.176)\,rad \qquad (39)$$

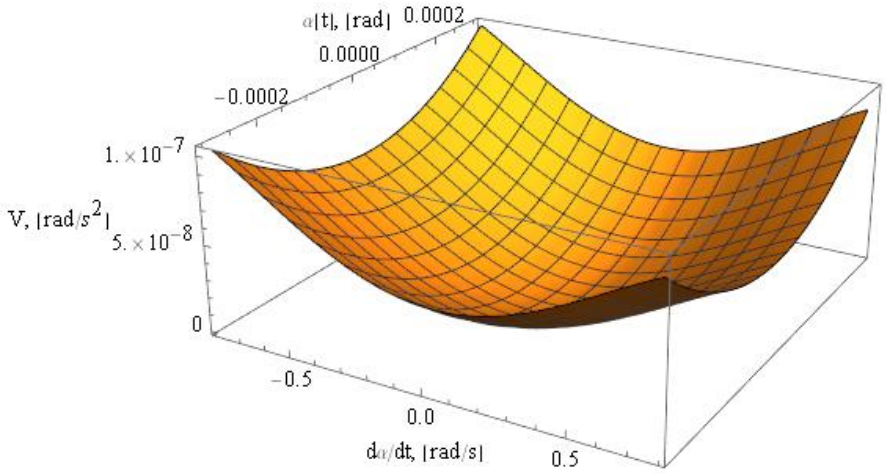

Fig. 12 The Lyapunov function (34) for the parameters (37)

Figs. 13 and 14 depict the stabilization of tether system during the implementation of the feedback control (31) for the parameters (37). In the first case, the initial point is located in the vicinity of the stable point $\alpha_s = 0.031\,rad$, and in the second case - in the vicinity of the unstable point $\alpha_{us} = 1.058\,rad$. Note that only in the first case (**Fig. 13 a**), the tether always remains stretched during the entire stabilization period.

a

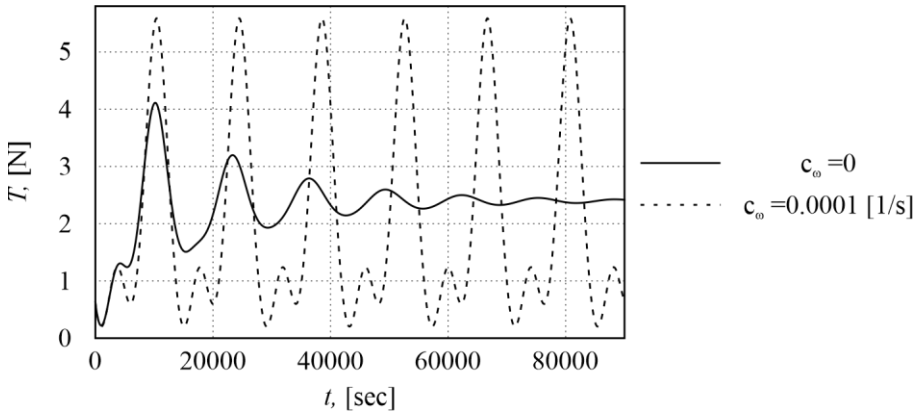

b

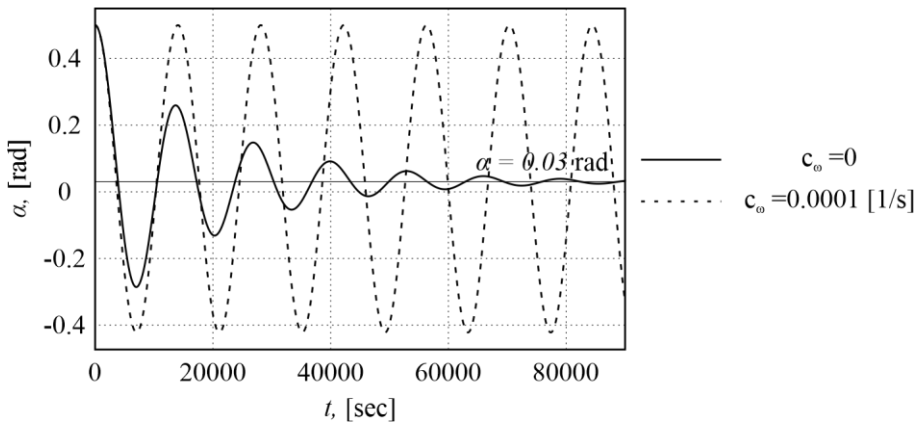

Fig. 13 **a** The tension force and **b** the angle of the tether deflection from the vertical for the end mass 5000 kg and parameters (37) under initial conditions $\alpha_0 = 0.5 rad,\ \dot{\alpha}_0 = 0$

a

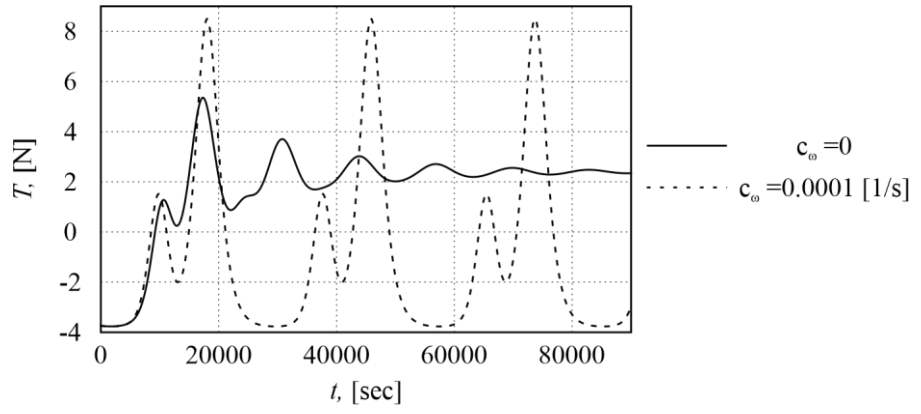

b

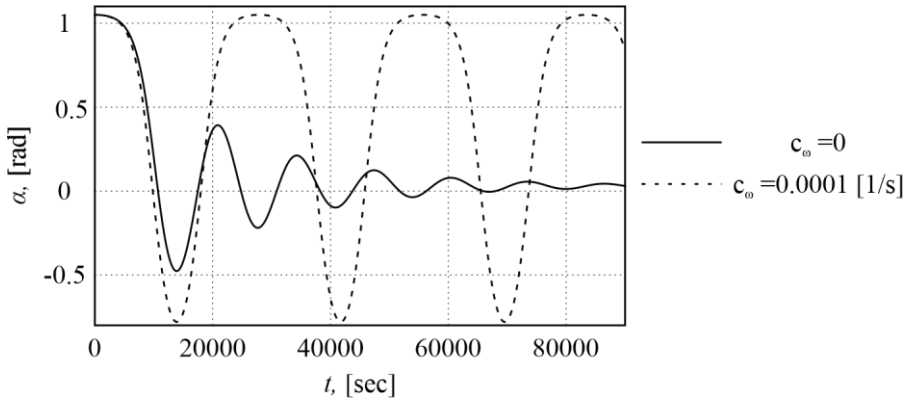

Fig. 14 a The tension force and **b** the angle of the tether deflection from the vertical for the end mass 5000 kg and parameters (37) under initial conditions $\alpha_0 = 1.05 rad,\ \dot{\alpha}_0 = 0$

6 Validation within an elliptic restricted three-body problem for the anchored tether

In this section, the results obtained above for the simplified circular mathematical models are validated by using an elliptic restricted three-body problem for the anchored tether. For this purpose, the motion equations of the tether system in Nechvile's variables are derived, using which the numerical simulation is performed to confirm the validity of the results obtained earlier.

6.1 Equations of motion in polar coordinates based on Nechvile's variables

We derive the planar motion equations of the end mass C in two gravitational fields of two primaries A_1 and A_2 (Mars-Phobos) in polar coordinates relative to the anchored point on the Phobos surface in terms of the restricted elliptic three-body problem [1, 29]. The distance between the two primaries is

$$r = \frac{p}{1 + e\cos f} \tag{40}$$

where p is the semilatus rectum, e is the eccentricity of the two-body orbit of the primaries, and f is the true anomaly. In the barycentre-centred synodic coordinate system, which rotates with the two primaries and using Nechvile's variables (ξ, η), the end mass motion can be described in dimensionless form as [1, 39]

$$\xi'' - 2\eta' = \frac{1}{1 + e\cos f}\frac{\partial \Omega}{\partial \xi} \tag{41}$$

$$\eta'' + 2\xi' = \frac{1}{1 + e\cos f}\frac{\partial \Omega}{\partial \eta} \tag{42}$$

where Ω is the potential function given by

$$\Omega = \frac{1}{2}\left(\xi^2 + \eta^2\right) + \frac{1-\mu}{r_1} + \frac{\mu}{r_2} \qquad \left(0 < \mu \le \frac{1}{2}\right) \tag{43}$$

$$r_1 = \sqrt{(\xi + \mu)^2 + \eta^2} \qquad r_2 = \sqrt{(\xi + \mu - 1)^2 + \eta^2} \tag{44}$$

where $(.)' = \frac{d}{df}(.)$ and $(.)'' = \frac{d^2}{df^2}(.)$; The dimensionless coordinates of the tether anchor point and the tether length are entered as follows

$$\sigma = \frac{a_x}{p}, \qquad \varepsilon = \frac{a_y}{p}, \qquad \lambda = \frac{l}{p} \tag{45}$$

Position of the end mass C relative to the anchored point in a polar reference frame (l, α) is defined by substituting the variables

$$\xi = \sigma - \lambda k \cos\alpha, \ \eta = \varepsilon - \lambda k \sin\alpha \tag{46}$$

where $k = 1 + e\cos f$.

Eqs. motion (41) and (42) in the polar reference frame (Fig. 1) are written as

$$\alpha'' + \Phi_\alpha = 0 \tag{47}$$

$$\lambda'' + \Phi_\lambda = -\bar{T} \tag{48}$$

where $\bar{T}$ is the dimensionless tether tension force,

$$\Phi_\alpha = -\frac{1}{\lambda k^2}\left[-\varepsilon\cos\alpha + \sigma\sin\alpha + 2e\lambda k \sin t(1+\alpha') - 2k^2\lambda'(1+\alpha') + \frac{(-1+\mu)(-\varepsilon\cos\alpha + (\mu+\sigma)\sin\alpha)}{\rho_1^3} + \frac{\mu(\varepsilon\cos\alpha - (-1+\mu+\sigma)\sin\alpha)}{\rho_2^3}\right] \tag{49}$$

$$\Phi_\lambda = -\lambda\alpha'(2+\alpha') - \lambda - \frac{1}{k^2}(2ek\lambda'\sin t - \sigma\cos\alpha - \varepsilon\sin\alpha) - \frac{1}{k^2}\left[-\frac{(-1+\mu)(-k\lambda + (\mu+\sigma)\cos\alpha + \varepsilon\sin\alpha)}{\rho_1^3} + \frac{\mu(-k\lambda + (-1+\mu+\sigma)\cos\alpha + \varepsilon\sin\alpha)}{\rho_2^3}\right] \tag{50}$$

where dimensionless distances between the primaries and the end mass

$$\rho_1 = \sqrt{(\mu + \sigma - k\lambda\cos\alpha)^2 + (\varepsilon - k\lambda\sin\alpha)^2} \tag{51}$$

$$\rho_2 = \sqrt{(-1 + \mu + \sigma - k\lambda\cos\alpha)^2 + (\varepsilon - k\lambda\sin\alpha)^2} \tag{52}$$

Assuming that the tether length is constant

$$l = const \to \lambda' = 0, \ \lambda'' = 0 \qquad (\lambda = \frac{l}{p}) \tag{53}$$

then from Eq. (48), the tether tension force is defined as

$$\bar{T} = \lambda\alpha'(2+\alpha') + \lambda - \frac{1}{k^2}(\sigma\cos\alpha + \varepsilon\sin\alpha) + \frac{1}{k^2}\left(-\frac{(-1+\mu)(-k\lambda + (\mu+\sigma)\cos\alpha + \varepsilon\sin\alpha)}{\rho_1^3} + \frac{\mu(-k\lambda + (-1+\mu+\sigma)\cos\alpha + \varepsilon\sin\alpha)}{\rho_2^3}\right) \tag{54}$$

The tether tension force (54) in dimensional form is written as

$$T = m\frac{G(m_1+m_2)p^2}{r^4}\left[\lambda\alpha'(2+\alpha') + \lambda - \frac{1}{k^2}(\sigma\cos\alpha + \varepsilon\sin\alpha) + \frac{1}{k^2}\left(-\frac{(-1+\mu)(-k\lambda + (\mu+\sigma)\cos\alpha + \varepsilon\sin\alpha)}{\rho_1^3} + \frac{\mu(-k\lambda + (-1+\mu+\sigma)\cos\alpha + \varepsilon\sin\alpha)}{\rho_2^3}\right)\right] \tag{55}$$

Taking into account the feedback control (31), the equations for the tether deflection angle (47) are rewritten as

$$\alpha'' + \Phi_\alpha = -c_\omega \frac{r^2}{\sqrt{G(m_1 + m_2)p}} \alpha' \qquad (56)$$

It should be noted that the Eq. (55) is exact for the simplified system of equations (41), (42). Estimating the accuracy of this formula requires building a more accurate mathematical model of the space tether system and comparing the simulation results, which is beyond the scope of this study.

6.2 Numerical simulations

The small eccentricity of the Mars-Phobos orbit ($e = 0.0151$) has no significant effect either on the oscillations of the anchoring tether system or on the tether tension force both with and without transverse displacement of the anchoring point, as Figs. 15 - 17 show. In all cases considered, the tether anchoring point is located on the Phobos surface without transverse displacement from the Ox axis, i.e. $a_y = 0$. Fig. 15 depicts the results of the numerical simulation without the feedback control ($c_\omega = 0$) and Fig. 16 with the feedback control ($c_\omega = 0.0001$) of the tether oscillation (31) . The tether length and the initial tether deflection angle are equal for this case, respectively

$$l_0 = 4500\,m,\ \alpha_0 = 0.5\,rad \qquad (57)$$

a

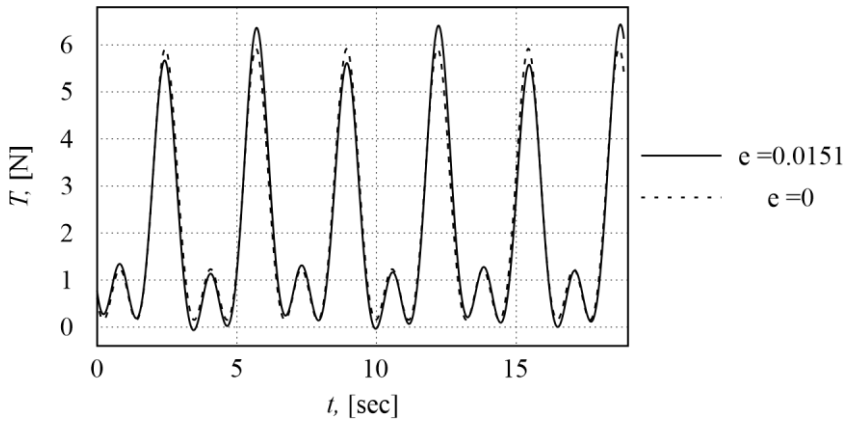

b

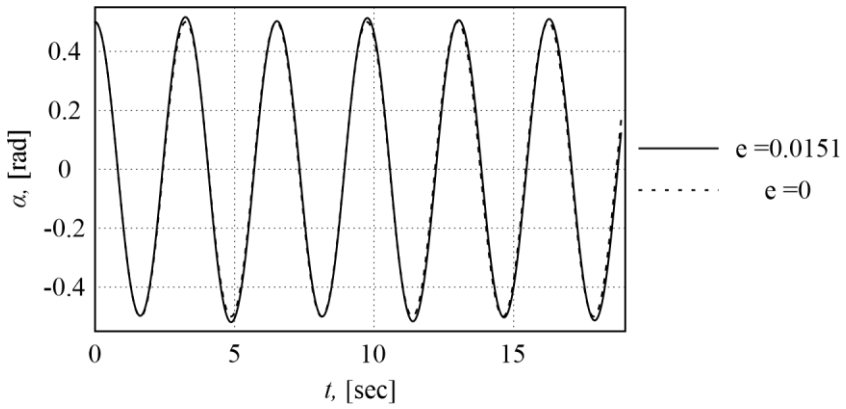

Fig. 15 **a** The tension force and **b** the angle of the tether deflection from the vertical for without control $c_\omega = 0$ the end mass 5000 kg and the tether 4500 m

a

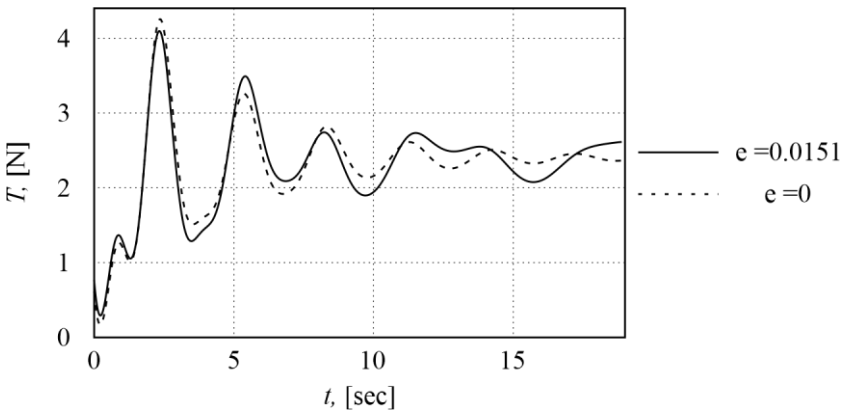

b

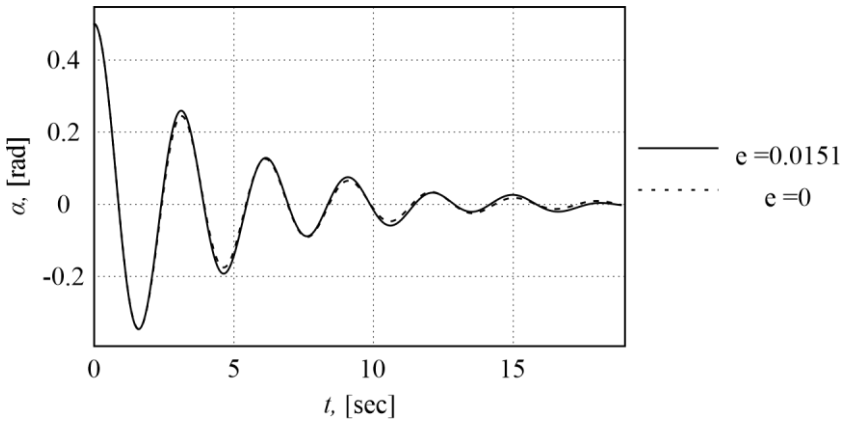

Fig. 16 **a** The tension force and **b** the angle of the tether deflection from the vertical with control $c_\omega = 0.0001$ for the end mass 5000 kg and the tether 4500 m

As can be seen from Figs. 16a and 17a, doubling the tether length ($l_0 = 9000\,m$) compared to the base value ($l_0 = 4500\,m$) leads to a fourfold increase in the maximum tension force.

a

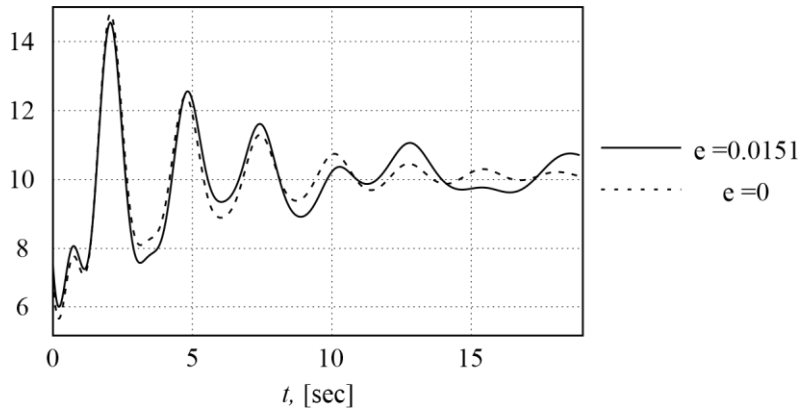

b

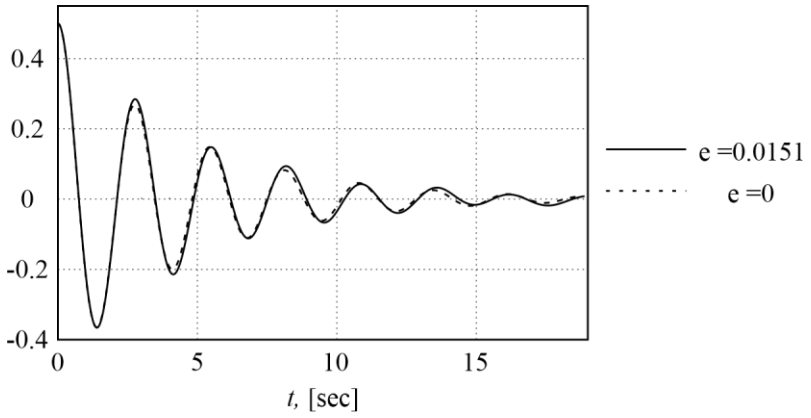

Fig. 17 a The tension force and **b** the angle of the tether deflection from the vertical with control $c_\omega = 0.0001$ for the end mass 5000 kg and the tether 9000 m

Numerical simulation shows that in the case of a small eccentricity, the proposed control still provides asymptotic stability.

7 Conclusions

The main results and conclusions about the possibility of implementing the conceptually new mission to study Phobos using the anchored tether system can be summarized as follows:

1. The planar motion equations the anchored tether under the Mars-Phobos L1 libration point have been derived for two cases: without taking into account eccentricity and using the Nechvile's variables with eccentricity. The tether has been considered as weightless and inextensible rod with an end mass. The energy integral, equilibrium positions have been found and phase portraits have been constructed for various anchored point locations on the Phobos surface.
2. Analytical formulas have been obtained to determine the tether tension, and it is shown that for the end mass of 5000 kg, this force is relatively small and does not exceed 20 N both in the static and dynamic state of the tether.
3. To reduce the amplitude of tether oscillations in the vicinity of the equilibrium position, the feedback control that can be implemented using thrusters has been proposed. It is shown that this control provides asymptotic stability of the tether system and this fact has been confirmed by numerical simulations.
4. Simplified mathematical models and analytical results have been substantiated and validated by numerical simulations based on more accurate models, taking into account the eccentricity of the Mars-Phobos orbit.

The proposed anchored tether system mission can be considered both as a separate mission and as a second phase of the PHLOTE mission, when the orbiter (end mass) first hangs at the L1 libration point, then the tether is anchored on the Phobos surface after which the anchored tether holds the orbiter. The second objective, which can be solved by the anchored tether system is an Orbiter-Phobos space elevator with a length of about 3-4 km. For a space elevator it is a very short length. This is the uniqueness of the Mars-Phobos L1 and L2 points of libration. Here it is relevant to note that in the Earth-Moon system the distance of the L1 libration point to the lunar surface is approximately 57,000 km, more than 15 thousand times more. Also and the length of the Earth-GEO space elevator is about 100 thousand km.

In continuation of this study, the proposed approach may be useful as other planet-moon systems and for other collinear libration points, for example L2 libration point. The development of the work is to study the behavior of the anchored system with an elastic-viscous tether, as well as to

study the possibility of building a space elevator Phobos - L1 libration point. The presented research is preliminary, which, quite possibly, will be developed and specified, if the interest in study of Phobos and other small celestial bodies will be increase. The proposed tether mission scene in the paper is not the only possible scene. Alternative schemas are quite possible and this may be the subject of the following works.

Acknowledgement

This study was supported by the Russian Science Foundation (Project No. 19-19-00085).

Compliance with ethical standards

Conflicts of interest. The author declares that he has no conflict of interest.

Data availability statement. The datasets generated during and/or analysed during the current study are available from the corresponding author on reasonable request.

References

1. Szebehely, V.: The Restricted Problem of Three Bodies. Academic Press Inc., New York (1967)
2. 20. Luo, T., Pucacco, G., Xu, M.: Lissajous and halo orbits inthe restricted three-body problem by normalization method. Nonlinear Dyn 101, 2629–2644 (2020). https://doi.org/10.1007/s11071-020-05875-1
3. Zotos, E.E.: Classifying orbits in the restricted three-bodyproblem. Nonlinear Dyn 82, 1233–1250 (2015). https://doi.org/10.1007/s11071-015-2229-4
4. Ferrari, F., Lavagna, M.: Periodic motion around librationpoints in the elliptic restricted three-body problem. Nonlinear Dyn 93, 453–462 (2018). https://doi.org/10.1007/s11071-018-4203-4
5. Woo, P., Misra, A.K.: Equilibrium points in the full three-body problem. Acta Astronaut. 99, 158–165 (2014). https://doi.org/10.1016/j.actaastro.2014.02.019
6. Biggs, J.D., Negri, A.: Orbit-attitude control in a circular restricted three-body problem using distributed reflectivity devices. J. Guid. Control. Dyn. 42(12), 2712–2721 (2019). https://doi.org/10.2514/1.G004493
7. Alessi, E.M., Sa´nchez, J.P.: Semi-analytical approach for distant encounters in the spatial circular restricted threebody problem. J. Guid. Control. Dyn. 39(2), 351–359 (2016). https://doi.org/10.2514/1.G001237
8. Aslanov, V.S. A splitting of collinear libration points in circular restricted three-body problem by an artificial electrostatic field. Nonlinear Dyn 103, 2451–2460 (2021). https://doi.org/10.1007/s11071-021-06226-4

9. Beletsky, V.V., Levin, E.V.: Dynamics of Space Tether Systems. Univelt Incorporated, San Diego (1993)
10. Levin, E.M.: Dynamic Analysis of Space Tether Missions.Univelt Incorporated, San Diego (2007)
11. Troger, H., Alpatov, A.P., Beletsky, V.V., Dranovskii, V.I.,Khoroshilov, V.S., Pirozhenko, A.V., Zakrzhevskii, A.E.:Dynamics of Tethered Space Systems. CRC Press, New York (2010)
12. Aslanov, V.S., Ledkov, A.S.: Dynamics of Tethered Satellite Systems. Woodhead Publishing, Cambridge (2012)
13. Williams, P. Deployment/retrieval optimization for flexible tethered satellite systems. Nonlinear Dyn 52, 159–179 (2008). https://doi.org/10.1007/s11071-007-9269-3
14. Williams, P., Blanksby, C., Trivailo, P.: Tethered planetarycapture maneuvers. J. Spacecr. Rocket. 41(4), 603–613 (2004). https://doi.org/10.2514/1.1024
15. Jung, W., Mazzoleni, A.P., Chung, J.: Nonlinear dynamicanalysis of a three-body tethered satellite system with deployment/retrieval. Nonlinear Dyn 82, 1127–1144 (2015). https://doi.org/10.1007/s11071-015-2221-z
16. Huang, P., Zhang, F., Chen, L., et al.: A review of space tether in new applications. Nonlinear Dyn 94, 1–19 (2018). https://doi.org/10.1007/s11071-018-4389-5
17. Yu, B.S., Xu, S.D., Jin, D.P.: Chaos in a tethered satellite system induced by atmospheric drag and Earth's oblateness. Nonlinear Dyn 101, 1233–1244 (2020). https://doi.org/10.1007/s11071-020-05844-8
18. Ledkov, A., Aslanov, V.: Evolution of space tethered system'sorbit during space debris towing taking into account the atmosphere influence. Nonlinear Dyn 96, 2211–2223 (2019). https://doi.org/10.1007/s11071-019-04918-6
19. Kumar, K., Yasaka, T.: Rotation formation flying of threesatellites using tethers. J. Spacecr. Rocket. 41(6), 973–985 (2004). https://doi.org/10.2514/1.14251
20. Cartmell, M.P., McKenzie, D.J.: A review of space tether research. Prog. Aerosp. Sci. 44(1), 1–21 (2008). https://doi.org/10.1016/j.paerosci.2007.08.002
21. Mashayekhi, M.J., Misra, A.K.: Optimization of tether-assisted asteroid deflection. J. Guid. Control. Dyn. 37(3), 898–906 (2014). https://doi.org/10.2514/1.60176
22. Aslanov, V.S. Prospects of a tether system deployed at the L1 libration point. Nonlinear Dyn 106, 2021–2033 (2021). https://doi.org/10.1007/s11071-021-06884-4

23. Sun, G., Zhu, Z. Fractional-order tension control law for deployment of space tether system. Journal of Guidance, Control, and Dynamics. 37(6), 2057–167 (2014). https://doi.org/10.2514/1.G000496
24. Kempton, K., Pearson, J., Levin, E., Carroll, J., & Amzajerdian, F., "Phase 1 Study for the Phobos L1 Operational Tether Experiment (PHLOTE)," End Report, NASA, 2018, pp.1-91. https://ntrs.nasa.gov/search.jsp?R=20190000916.
25. Vaisberg, O.L., Kogan, A.Yu., and Levin, E.M. Tethered Systems for the Exploration of the Magnetospheres of the Earth and Mars. Preprint of the Institute for Space Research of the USSR Academy of Sciences, No. 1470, 1988, (in Russian).
26. Radley, Charles F. "Lunar Space Elevator Infrastructure." Journal of Geoethical Nanotechnology 7.2 (2012): 13-19. https://www.terasemjournals.org/GNJournal/GN0702/GN0702.html
27. Li, G., Zhu, Z.H. Model predictive control for electrodynamic tether geometric profile in orbital maneuvering with finite element state estimator. Nonlinear Dyn 106, 473–489 (2021). https://doi.org/10.1007/s11071-021-06869-3
28. Wen, H., Huang, L., Xu, S. et al. Angular velocity observer for space tether exploiting non-singular dynamics and vector measurements. Nonlinear Dyn 104, 399–410 (2021). https://doi.org/10.1007/s11071-021-06211-x
29. Zhang, F., Sharf, I., Misra, A., & Huang, P. On-line estimation of inertia parameters of space debris for its tether-assisted removal. Acta Astronautica, 107, 150-162 (2015). http://dx.doi.org/10.1016/j.actaastro.2014.11.016
30. Li, G., Zhu, Z.H. On libration suppression of partial space elevator with a moving climber. Nonlinear Dyn 97, 2107–2125 (2019). https://doi.org/10.1007/s11071-019-05108-0
31. Zhang, F., Huang, P. A novel underactuated control scheme for deployment/retrieval of space tethered system. Nonlinear Dyn 95, 3465–3476 (2019). https://doi.org/10.1007/s11071-019-04767-3
32. Krupa, M., Poth, W., Schagerl, M. et al. Modelling, Dynamics and Control of Tethered Satellite Systems. Nonlinear Dyn 43, 73–96 (2006). https://doi.org/10.1007/s11071-006-0752-z
33. Ferreira, A.F.S., Moraes, R.V., Prado, A.F.B.A. et al. A mathematical study of the tethered slingshot maneuver using the elliptic restricted problem. Nonlinear Dyn 102, 1585–1609 (2020). https://doi.org/10.1007/s11071-020-05992-x

34. Jung, W., Mazzoleni, A.P. & Chung, J. Dynamic analysis of a tethered satellite system with a moving mass. Nonlinear Dyn 75, 267–281 (2014). https://doi.org/10.1007/s11071-013-1064-8
35. Zhu, G., Lu, K., Cao, Q. et al. Dynamic behavior analysis of tethered satellite system based on Floquet theory. Nonlinear Dyn (2022). https://doi.org/10.1007/s11071-022-07466-8
36. Yu, B.S., Ji, K., Wei, Z.T. et al. In-plane global dynamics and ground experiment of a linear tethered formation with three satellites. Nonlinear Dyn (2022). https://doi.org/10.1007/s11071-022-07403-9
37. Basilevsky, A. T., C. A. Lorenz, T. V. Shingareva, J. W. Head, K. R. Ramsley, and A. E. Zubarev. "The surface geology and geomorphology of Phobos." Planetary and Space Science 102 (2014): 95-118. http://dx.doi.org/10.1016/j.pss.2014.04.013
38. Lucchetti, A., Cremonese, G., Pajola, M., Massironi, M. and Simioni, E., 2015. New simulation of Phobos Stickney crater.
URI: http://hdl.handle.net/20.500.12386/26076
URL: https://www.hou.usra.edu/meetings/lpsc2015/pdf/1420.pdf
39. Markeev, A. P.: Libration Points in Celestial Mechanics and Astrodynamics, Nauka, Moscow [in Russian] (1978)